

Self-configurable cyber-physical intrusion detection for smart homes using reinforcement learning

Ryan Heartfield, *Member, IEEE*, George Loukas, Anatolij Bezemskij, Emmanouil Panaousis, *Member, IEEE*

Abstract—The modern Internet of Things (IoT)-based smart home is a challenging environment to secure: devices change, new vulnerabilities are discovered and often remain unpatched, and different users interact with their devices differently and have different cyber risk attitudes. A security breach’s impact is not limited to cyberspace, as it can also affect or be facilitated in physical space, for example, via voice. In this environment, intrusion detection cannot rely solely on static models that remain the same over time and are the same for all users. We present MAGPIE, the first smart home intrusion detection system that is able to autonomously adjust the decision function of its underlying anomaly classification models to a smart home’s changing conditions (e.g., new devices, new automation rules and user interaction with them). The method achieves this goal by applying a novel probabilistic cluster-based reward mechanism to non-stationary multi-armed bandit reinforcement learning. MAGPIE rewards the sets of hyperparameters of its underlying isolation forest unsupervised anomaly classifiers based on the cluster silhouette scores of their output.

Experimental evaluation in a real household shows that MAGPIE exhibits high accuracy because of two further innovations: it takes into account both cyber and physical sources of data; and it detects human presence to utilise models that exhibit the highest accuracy in each case. MAGPIE is available in *open-source format*, together with its evaluation datasets, so it can benefit from future advances in unsupervised and reinforcement learning and be able to be enriched with further sources of data as smart home environments and attacks evolve.

Index Terms—Intrusion Detection System, Cyber-physical attacks, Smart Home, Reinforcement Learning.

I. INTRODUCTION

The mass adoption of IoT technology in smart homes has made them attractive targets to cyber threats, from unlocking doors and eavesdropping on occupants through their own cameras to hijacking voice-controlled personal assistant devices. Commercial trends for protecting against such threats revolve mainly around preventive measures, such as encryption or two-factor authentication, but the assumption that these measures are sufficient is not well-grounded [1], as vulnerabilities for IoT devices are discovered and exploited routinely despite them. In environments involving multiple devices of varying levels of trustworthiness and likely inter-dependencies between them, such as those found in smart homes, it makes sense to try to detect security breaches when they occur.

Intrusion detection is not new to the IoT [2]. In fact, several solutions have been proposed specifically for smart city and industrial IoT environments [3, 4]. Smart homes,

however, present unique challenges with very specific requirements that can make generalist approaches unsuitable. They consist of multiple commercial off-the-shelf (COTS) devices, each often using a different network protocol, sometimes directly connected to the household’s Wi-Fi router, other times connected indirectly through a specialised hub, and usually in an encrypted format. Users tend to develop their own automation rules that virtually link otherwise unconnected devices, including external ones, in unpredictable ways.

Furthermore, new vulnerabilities are discovered on a daily basis, and it is unrealistic to expect a smart home intrusion detection system to always be aware of all threats. Additionally, cyber-physical attacks (i.e., cybersecurity breaches that have adverse physical impact in the form of unauthorised, delayed, incorrect or altogether prevented actuation, or in the form of physical privacy breaches [5]) can affect domestic life and a person’s behaviour and psychological state in their own home [6]. Different users have different risk attitudes in this context and would wish to configure differently any security measures protecting their smart home. Finally, in most cases, the cost of COTS smart home devices is relatively low, so any added security provision introduced should not itself require expensive equipment to run on.

We have addressed the above requirements by designing and implementing MAGPIE (**mon**itoring **ag**ainst **cyber**physical threats), an intrusion detection system (IDS) prototype for smart homes subjected to a variety of cyber-physical security threats, both known and (at the time of execution) unknown. For a smart home IDS to be effective against unknown attacks and in changing conditions, it must be able to adapt. We argue that the configuration of an unsupervised classifier can be adapted continuously via reinforcement learning as it provides dynamic capability to continuously adapt an IDS configuration via conceptualisation of “actions” within a detection adaptation process, guided by learning the relationships between anomalous and normal cyber-physical behaviour in the environment. The challenge here is that an unsupervised IDS system cannot know the groundtruth (i.e., whether there really was an attack or not); thus, reinforcement learning cannot reward a classifier’s specific set of hyperparameter values based on the groundtruth. However, in most attacks on a smart home, the less confident a classifier is, the more inaccurate it is in practice. Based on this observation, MAGPIE applies a simple idea for the first time: the reward function of reinforcement learning on an unsupervised classifier’s hyperparameters can be based on the classifier’s own confidence in its output, as expressed through its cluster silhouette scores. We have tested and confirmed the validity of this idea experimentally.

All authors are with the School of Computing and Mathematical Sciences, University of Greenwich, Old Royal Naval College, SE10 9LS, London, UK. E-mails: {r.heartfield, g.loukas, a.bezemskij, e.panaousis}@gre.ac.uk.

In addition, MAGPIE introduces three more innovations to ensure its practicality in a household, including taking into account users' risk tolerance, human presence and cyber-physical sources of data. In summary, MAGPIE implements the following contributions:

- Ability to **continuously adapt unsupervised smart home threat detection to changing conditions**. MAGPIE self-adapts by applying reinforcement learning on the unsupervised classifier's hyperparameters based on a probabilistic reward function without an a priori model or knowledge of the household configuration.
- Experimental evaluation with **both cyber and physical sources of data**. From a threat monitoring perspective, the physical impact of some security breaches constitutes an opportunity because, in conjunction with traditional cyber sources of data, it can provide valuable information about the system's security state.
- **Self-configuration based on automated inference of human presence**. In a smart home, the models of what is normal or not depend on human presence. For example, a voice-activated action being triggered when a human is present carries different significance to one triggered in the absence of a human.

We provide MAGPIE in open-source format for installation on a low-cost Linux computer, such as a Raspberry PI*.

II. RELATED WORK

Traditionally, the vast majority of IoT security research applicable to current smart homes has focused on authentication and access control [7, 8, 9]. Lately, there has been a growing body of work tackling the challenge of detection, whether knowledge-based (utilising signatures of known attacks) or behaviour-based (detecting deviation from normal behaviour).

A. Knowledge-based smart home IDS

Anthi et al. [10] utilised standard machine learning classifiers, such as naive Bayes, to categorise IoT activity as normal or malicious. The features used were limited to network traffic and were similar to those used for non-IoT traffic, including timestamp, destination IP, protocol and packet size. In [11], the authors specifically classified which types of attacks have occurred based on supervised learning. This information can be very useful for triggering response mechanisms, but it is only applicable for known attacks and requires an extensive period of training under attack conditions (two weeks in the cited paper), which may be impractical for a household's smart home network.

Brun et al. [12] focused on detecting attacks on smart home IoT gateways. They employed a deep learning-based approach using dense random neural networks. However, the attacks utilised in the performance evaluation were simple TCP SYN denial of service attacks, which were shown to be almost as easily detectable by a simple threshold detector. Moustafa et al. [13] started with generalist datasets for botnets but enriched

them with simulated IoT sensor data. Their learning approach was based on an Adaboost ensemble of decision trees, naive Bayes and artificial neural networks. However, the approach has not been evaluated with actual smart home devices and does not account for changes in usage patterns over time.

Nobakht et al. [14] employed a method based on software-defined networking technology, specifically OpenFlow, for providing modularity in intrusion detection for smart homes. Their experimental evaluation however was on a single light bulb, and the technique itself was based on known signatures of attacks, which limited its wider potential for large smart home setups or previously unseen attacks.

Trimananda et al. [20] addressed the specific challenge of information inference attacks in smart homes. Their tool is able to automatically extract packet-level signatures for device events based only on packet lengths and durations to predict which device is activated. Although very useful in anomaly detection, this approach has not yet been employed in this fashion. Additionally, it is naturally limited to attacks related to the unauthorised activation of devices.

B. Behaviour-based smart home IDS

Wan et al. [21] introduced IoTArgos, which in addition to supervised classification of the data communications of different smart home devices, has a "second stage" of detection using unsupervised learning for unknown attacks. This is a meaningful direction and has been evaluated on a wide range of COTS smart home devices. However, the cost of the two detection stages has not been evaluated, and the method does not take into account the presence of the user or the smart home's changing conditions.

A very interesting idea was developed in EclipseIoT [22], which in addition to authentication and access control, features an early detection provision based on canary files. These are forged files with enticing names (e.g., "SmartLock.py") placed amongst genuine ones. Modification of a canary file is an indication of unauthorised access.

Procopiou et al. [15] proposed a lightweight algorithm based on forecasting and chaos theory to identify flooding and DDoS attacks launched by compromised smart home devices. For every time-series behaviour collected, a forecast is generated, and the error of the forecast against the actual value is assessed by the Lyapunov exponent to determine if an attack has occurred. The evaluation conducted in NS-3 simulation involved low-rate and flooding attacks, but the method has not been extended beyond availability threats.

Novak et al. [16] proposed an intrusion detection technique that focuses on identifying unusually short and unusually long activities based on self-organising maps. While the approach of taking into account the length of activities proved to be useful, it is not sufficient by itself and can lead to considerable false positives.

Ramapatruni et al. [17] employed a hidden Markov model-based approach that learns what is normal in a smart home. In terms of context, if the user is recognised as being out (based on their mobile device's Wi-Fi connectivity), then any activity related to doors will result in an abnormal state. A strength of

*The code and datasets used here are provided at <https://github.com/isecongreenwich/magpie>

Table I: Limitations in existing intrusion detection research for IoT and Smart homes Vs. MAGPIE

IDS	Cyber sources	Physical sources	Self-configuration	Testbed
[10]	IP	X	X	Laboratory
[12]	IP	X	X	Laboratory
[13]	IP	X	X	UNSW-NB 15, NIMS datasets
[15]	IP	X	X	Simulation
[16]	ZigBee	X	X	Simulation
[17]	IP	Sensor readings (HTTP API)	X	Smart home testbed
[18]	IP	X	X	Laboratory
[19]	IP, WiFi, BLE	X	X	Laboratory
[11]	IP	X	X	Smart home testbed
[20]	IP	X	X	Smart home testbed
[14]	IP	X	X	Smart home testbed
[21]	IP	X	X	Smart home testbed
MAGPIE	Modular (IP, ZigBee, WiFi tested)	Modular (RF, Audio tested)	Continuous*	Real household

* via RL-based hyperparameter adaptation and Human presence inference

204 this work is that it can take into account the traffic generated
 205 by several diverse sensors, but it has been evaluated only in
 206 simulations in the form of artificial state changes.

207 Yamauchi et al. [23] expanded consideration of the user by
 208 modelling user behaviour as a sequence of events, including
 209 the operation of IoT devices and other behaviour monitored
 210 by sensors. Their method learns sequences of events for a
 211 predefined set of conditions and detects attacks by comparing
 212 the sequences of events, including the current operation, with
 213 the learned sequences. This work was extended in [18] and
 214 compared with a technique based on a hidden Markov model.
 215 It was tested on four users using smart home devices, but in a
 216 laboratory setting. Naturally, any legitimate behaviour that had
 217 not been previously observed would erroneously be flagged as
 218 anomalous.

219 C. Critique of related work

220 We observe that there is a wide variety of machine learning
 221 classifiers utilised in the literature, but there has been no
 222 emphasis on allowing configuration of intrusion detection
 223 beyond the design stage or based on the user’s preferences.
 224 In addition, existing smart home IDSs have largely ignored
 225 the fact that cyber attacks in smart homes have an observable
 226 physical impact, which can be useful in detection. Finally, with
 227 the exception of [23], human presence has not been taken into
 228 account in smart home IDS research, although normal IoT
 229 device and network activity differ when the users are at home
 230 versus when they are not. In Table I, we provide an overview
 231 of the existing literature on intrusion detection approaches and
 232 MAGPIE, and in the following sections, we present, in detail,
 233 how MAGPIE addresses all four limitations.

234 III. MAGPIE DESIGN

235 Figure 1 summarises the MAGPIE architecture. Its *collec-*
 236 *tion phase* captures and decodes the data coming from cyber
 237 (computation, communication) or physical feeds (e.g., audio,
 238 signal strength). It can dynamically activate or deactivate
 239 interfaces and decode the corresponding raw feeds, such as
 240 sensor readings or network datagrams.

241 Smart homes generate large volumes of usually encrypted
 242 data [24] that may differ considerably between different envi-
 243 ronments. In the *transcription phase*, MAGPIE considers only
 244 meta-data that are consistent across different smart homes.
 245 We argue that alternative approaches, such as authenticated

246 and encrypted device API queries or passive interception
 247 of content with decryption keys, would render the defence
 248 mechanism a single point of failure and a target for attack.
 249 Moreover, by reading only smart home network communica-
 250 tion flow meta-data, MAGPIE is better positioned to preserve
 251 privacy. MAGPIE extracts meta-data streams (MDS) based on
 252 specific interface datastream parsing logic (e.g., communica-
 253 tion/application/sensor protocol) (Figure 2). Rolling window-
 254 based parser extraction and buffering allow appropriate per-
 255 formance and volume of data samples for processing. After
 256 aggregating, statistical information on the extracted meta-data
 257 features, such as the mean, standard deviation, min and max
 258 of sample frequency, content/message type, size, length, delay
 259 and flow direction, is considered. We define the delay meta-
 260 data feature as the inter-arrival rate in milliseconds between
 261 packets/frames for the same source-destination message type
 262 pairs.

263 Table II shows the volume and inter-arrival rate for samples
 264 collected in a 5-min window in our smart home testbed during
 265 periods of relatively low occupant activity with an aggregate
 266 average sample inter-arrival rate of 0.49 s and average sample
 267 volume of 3456, with extremes of under 1 ns between input
 268 samples in some cases. On the basis of these observations,
 269 it is clear that analysis on datastream samples in real time,
 270 without windowing and buffering, is impractical on a resource-
 271 constrained platform. Moreover, it may prove impractical to
 272 offload such volumes of data due to file size, upstream network
 273 bandwidth saturation and throttling [25].

Table II: Datastream sample inter-arrival time in seconds with no smart home occupant present (5-min capture)

Datastream	Samples	Avg.	Min	Max	Stdev.
IP	569	0.5369	0.00002	4.0338	0.9539
WiFi	3555	0.0892	0.0008	0.2048	0.1023
Sound	12465	0.0240	0.0121	0.0718	0.0146
Zigbee	390	0.7848	0.0002	5.3879	1.3882
RF	300	1	1	1	0

274 As part of windowing, a synchronised “end of window”
 275 datastream buffer is the stage where a parsing instance should
 276 initiate feature extraction, interpolation, discretisation and gen-
 277 eration of statistical data (Figure 2). The datastream window in
 278 the buffer is then forwarded to a parsing logic and interpolation
 279 phase, where meta-data extraction and feature interpolation
 280 are performed on raw datastreams and are enumerated with
 281 protocol mapping identifiers (e.g., addressing, data type). The

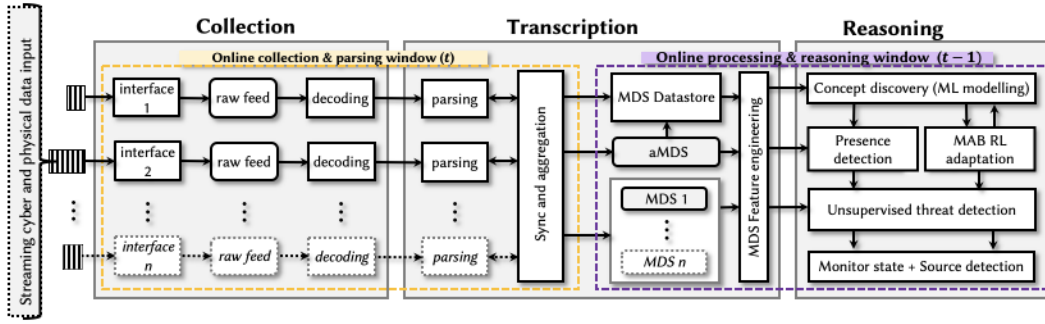
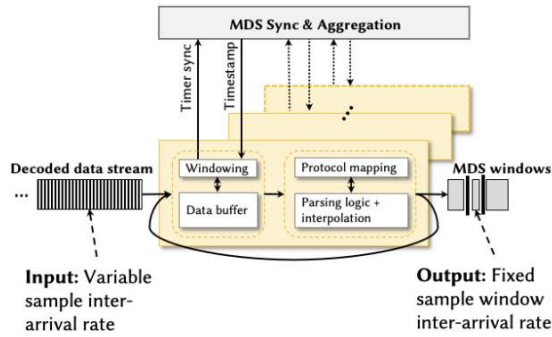
Figure 1: The *MAGPIE* architecture

Figure 2: Parsing datastreams with variable inter-arrival rate

n is the number of samples (or data set size) per window t and δ represents the computation of distinct source-destination pairs by connection address, port and message type. For physical data sources (RF and Audio), the computational complexity is $O(n)$. For training, the individual linear time complexity for each isolation forest model is $O(\zeta\psi \log\psi)$ [26]. During real-time detection, the computational complexity of each isolation forest model is $O(n\zeta \log\psi)$. From a technical implementation perspective, *MAGPIE*'s processing efficiency is achieved by running parallel transcription processes for each data source and anomaly model. During the course of testing on a Raspberry Pi3, on average, the transcription phase did not exceed 1 s for each monitoring window t or 2.5 s for the end-to-end processing phases (collection, transcription and reasoning) at peak loads across five data sources.

output is the MDS window feed, which is forwarded for storage to the MDS datastore to fuse data points across all MDS datastreams into an aggregated sample (aMDS). The datastore serves as a data historian for anomaly detection training (e.g., concept discovery) and captures snapshots of MDS data samples used in reinforcement learning-based adaptation (Section III-A). The aMDS fusion extracts common statistical features across all MDS feeds, which are later used to train a presence inference function within the smart home. The aMDS dataset combines common features across MDS feeds to generate a single feature-vector sample per window t for presence inference (whilst each MDS can have different sample rates for t) by omitting source-destination address and message type pairs for network data sources and compressing some physical MDS input. The average, mode, cumulative sum and standard deviation metrics are obtained for each feature extracted across each MDS feed.

The real-time threat monitoring latency is the window buffering latency plus the reasoning engine's prediction latency. All received MDS feeds are processed, interpolated, normalised and scaled in real time during each monitoring window interval. This process provides the required feature structures for concept discovery training data to learn "normal" behaviour and generate an independent anomaly detection model for each interface. Note that the complexity of the *MAGPIE* transcription phase is variable based on the cyber or physical data source, the sample rate and whether the data source is connection-oriented. For example, for network data sources (IP, WiFi, ZigBee), the computational complexity of the end-to-end parsing logic and interpolation is $O(n^\delta)$, where

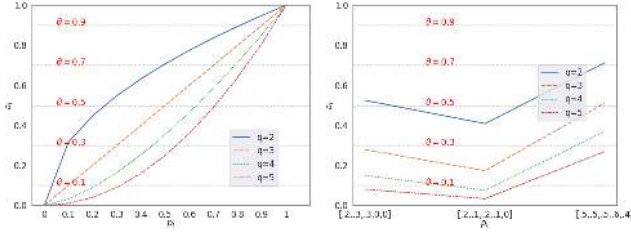
A. Reasoning

MAGPIE employs (i) real-time unsupervised anomaly detection, (ii) adaptation based on reinforcement learning, and (iii) model selection based on human presence inference.

1) *Unsupervised anomaly detection*: The first building block of *MAGPIE*'s reasoning is the real-time detection of anomalies on individual interfaces. Here, supervised machine learning techniques are impractical because attack dataset labelling is unlikely to apply across households with different system configurations and different automation rules defined by their users. Let us consider the general case of an MDS feed $k \in [1, K]$ monitored during time window t .

During that time window, M samples are collected, A of which are classified by an anomaly detection process as abnormal and N of which are classified as normal, for example, based on an isolation forest [26] classifier, one-class support vector machines [27] or support vector data description [28]. We denote by A_t (resp. N_t) the number of *abnormal* (resp. *normal*), according to *MAGPIE*, samples investigated during time window t . Therefore, regardless of the choice of anomaly classifier used, for each MDS feed k in window t , we denote by $A_{k,t}$ (resp. $N_{k,t}$) the number of anomalous (resp. normal) samples found in feed k during time t . We then define the *anomaly ratio* $p_{k,t}$ as $p_{k,t} = \frac{A_{k,t}}{A_{k,t} + N_{k,t}}$.

Extending this approach across all feeds, we derive an aggregate *anomaly score* a_t for time window t . We have



(a) All models p_t equal or 1 model (b) Variable p_t across all models ≥ 0.1 with all others = 0

Figure 3: q parameter anomaly score bias example

chosen

$$a_t = \left(\frac{\sum_{k=1}^K p_{k,t}^q}{\sum_{k=1}^K p_{k,t}} \right)^{\frac{1}{q-1}} \quad (1)$$

This transformation is required because different data sources can exhibit highly variable behaviour, and a single source's anomaly score is not a reliable means for determining an attack state. As described in [29], a simple approach, such as a weighted sum, cannot deliver reliable results because individual anomaly scores are typically contradictory. Therefore, we use the aggregate anomaly score a_t to address skewness. As square roots are commonly used for left skewness while cube roots are used for right skewness, the introduction of q allows for flexibility in the transformation. In practice, the control parameter q configures a higher, lower or balanced anomaly score bias across the ensemble. Favouring higher or lower scoring bias, however, can have an adverse effect on the anomaly score threshold θ defined by the smart home occupants for when to report a suspected attack. For example, in Figure 3, we demonstrate how an ensemble of five data sources, as in our experiments, can affect the detection accuracy if the user has defined a specific θ when q is too low or too high. For the top graph in Figure 3, for each aggregate score a_t (where all models are equal to the same p_t , or one model $p_t > 0$ with all other models $p_t = 0$), we show that depending on the user's defined θ , the value of q results in higher false positives or false negatives. For balanced accuracy, in this case, $q = 3$ is an optimal configuration for an ensemble of five anomaly models. In the bottom graph in Figure 3, we provide three general cases with variable anomaly model ratio scores p_t . If an occupant defines $\theta = 0.3$ as their attack threshold, then $q = 2$ would result in more false positives, while $q = 5$ would result in more false negatives. Thus, a middle-ground q parameter is preferable (again, in this example with five models, $q = 3$). Consequently, q must be increased or decreased as the number of data sources changes (where a minimum of two data sources, e.g., cyber + physical, is assumed and $K \geq 2$). In our experiments, we found that a middle-ground value, i.e., $q = \lceil \frac{K}{2} \rceil$, is appropriate and can be set automatically.

As $p_{k,t} \in [0, 1]$, this conveniently ensures that $a_t \in [0, 1]$. Thus, according to (1), the higher the $q \in [2, \text{inf}]$ is, the more important one abnormal feed is to the overall anomaly score. As discussed, we have found experimentally that $q = 3$ provides a good balance between ensuring that the overall

score does not unduly fluctuate between excessively high values caused by small numbers of anomalous MDS feeds (e.g., one cyber and one physical interface) or excessively low values caused by large numbers of normal MDS feeds (e.g., ten cyber/physical interfaces). Thus, for simplicity, equation

$$(1) \text{ becomes } a_t = \sqrt{\frac{\sum_{k=1}^K p_{k,t}^3}{\sum_{k=1}^K p_{k,t}}}.$$

Finally, the anomaly score is interpreted as an overall monitoring state \mathcal{S}_t for the smart home, abnormal (if $a_t > \theta$) or normal (if $a_t < \theta$), based on an anomaly score threshold $\theta \in [0, 1]$, which is selected by the occupants.

In practice, θ is a threshold that represents the *risk profile* of the household. For example, a very high value, such as $\theta = 0.9$, would mean that the household would not want to be warned unless there are multiple strong indications of anomalies (risk-seeking profile). Intuitively, this is a household that would prefer to minimise false positives at the expense of a greater number of false negatives. In MAGPIE, a global θ threshold represents a single configuration parameter that occupants configure for attack detection. While model-specific θ definitions would increase the flexibility and control for the user, it would also increase the configuration complexity. First, users would require technical expertise to determine which θ to use for each data source, as it is unrealistic to assume a priori knowledge on the mapping between which θ values would bias one source over another. Furthermore, considering a preference for cyber or physical attack detection in cyber-physical IDS, it may be ineffective to define specific θ values that bias one cyber or physical source over another, specifically because attacks against either may be initiated via cyber or physical space [5]. By comparison, a global θ definition specifies a required threshold for an aggregate anomaly alert to be considered significant enough to be a substantive attack, regardless of whether the attack source is cyber or physical.

Further, to improve the processing of MDS samples as timeseries data, a sliding window of MDS samples is defined per MDS feed. The sliding window enables the anomaly score ratio calculation to take into account a previous window (or windows) of MDS activity.

2) *Adaptation based on reinforcement learning*: A newly installed smart home's dataset is typically free from contamination. After some time, however, the MDS datastore is likely to contain adversarial data samples from historic attacks or compromised devices. Therefore, it is important to adapt the learning process to cope with adversarial datapoints. This requirement is addressed naturally in certain unsupervised learning approaches through the application of contamination hyperparameters that adjust the decision threshold used for anomaly detection. Furthermore, what is considered normal in a household can change continuously as devices are added, removed or updated and as people add or remove automation rules or simply change how they use the devices. Therefore, changes in the datastream distribution require continuous adaptation of the anomaly detection threshold. Concept discovery is unique for each smart home, even for households with identical smart home configurations, because the network, sensor and actuation activity depends on the human factor [30]. Therefore, an unsupervised anomaly detection model

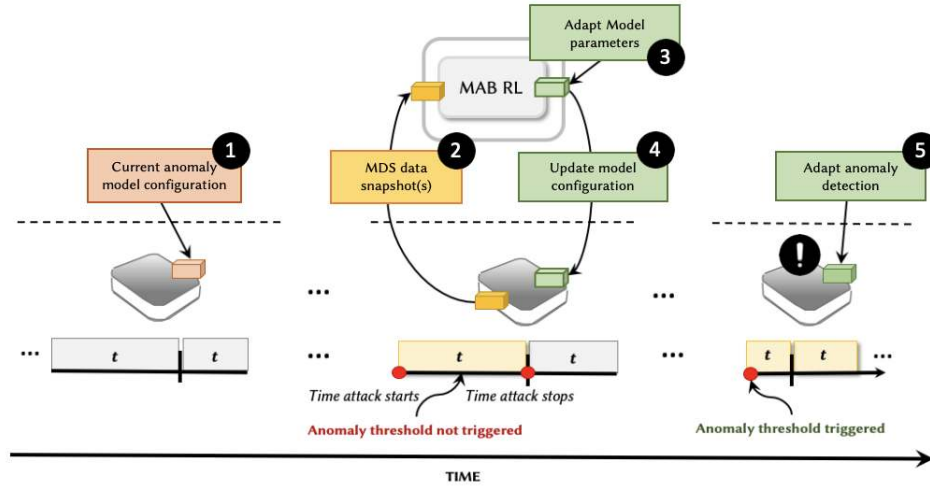


Figure 4: MAGPIE's reinforcement learning for threat detection re-configuration

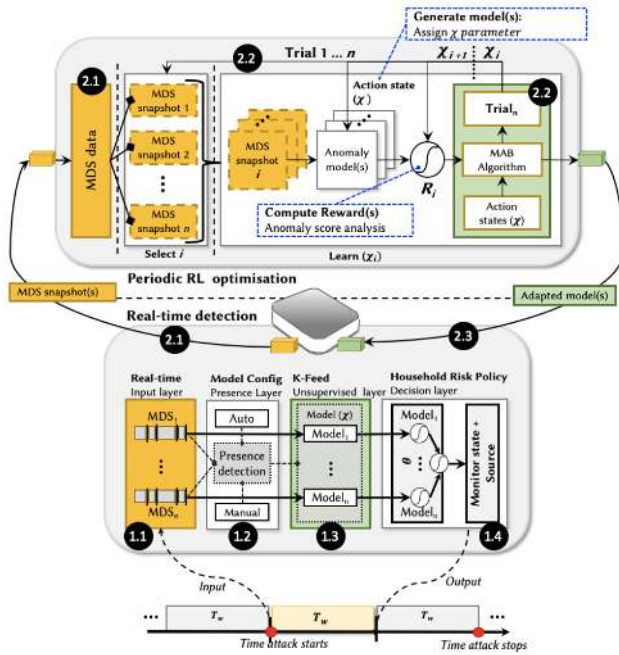


Figure 5: MAGPIE Reasoning Engine overview

449 developed for one smart home is not portable to another.
 450 As it is generally infeasible to obtain a priori knowledge
 451 of the correct contamination level, we propose the use of
 452 reinforcement learning to continuously update the anomaly
 453 classifier's hyperparameters.

454 The reinforcement learning mechanism in MAGPIE re-
 455 cursively explores and exploits detection reward feedback
 456 across different anomaly classifier configurations, where a
 457 single action-state (i.e., the anomaly classifier hyperparameter
 458 configuration) is selected during each step. The process treats
 459 the continuous capture and analysis of each MDS snapshot
 460 as an adversarial multi-armed bandit (MAB) environment
 461 [31, 32] because the composition of an individual dataset
 462 snapshot collected and analysed by MAGPIE (e.g., in terms of
 463 volume and data points) is continuously changing during real-
 464 time operation. This approach enables the anomaly detection

465 to adapt to previously unseen data and to identify legitimate
 466 changes that occur in the environment that are expected to
 467 stabilise over time, whereas attack anomalies remain distinct
 468 because of their sparse occurrences.

469 For each MAB iteration, we define a probabilistic reward
 470 feedback based on the cluster silhouette scores of the anomaly
 471 detection results generated for each analysed dataset snapshot.
 472 In practice, the reinforcement learning process rewards the
 473 action-states (e.g., bandit arms) that reduce uncertainty in its
 474 own decision. Below, we describe the bandit environment,
 475 action-state parameters and reward generation algorithm:

476 **[Bandit environment]:** Defined as an adversarial bandit
 477 [33], where for each MAB action-state parameter iteration 1
 478 to N (where N is the step horizon for a bandit episode), MDS
 479 data snapshot $i \in [J]$ is selected at random, and $[J]$ is the set
 480 containing all current MDS feed datastore snapshots.

481 **[Action-state parameter]:** The bandit arms are defined by
 482 the *anomaly model contamination hyperparameter* χ , which
 483 corresponds to the proportion of outliers in snapshot i used
 484 for anomaly modelling. The χ hyperparameter controls the
 485 anomaly detection decision threshold based on the anomaly
 486 detection classifier. For example, for our MAGPIE implemen-
 487 tation, χ controls the decision threshold of an isolation forest
 488 classifier based on the decision function described in [26].

489 **[MAB reward generation algorithm 1]:** The reward logic
 490 is as follows: for a given window $t \in [1, T]$, each MAB iter-
 491 ation corresponds to a given action-state (i.e., contamination
 492 hyperparameter) χ . We define $a_{t,\chi}$ as the anomaly score value
 493 of time window t for a contamination hyperparameter χ , and
 494 we denote \vec{a}_χ as the vector of all anomaly scores for χ for all
 495 the different time windows t .

496 Next, using K-means clustering with the Euclidean distance,
 497 we generate two clusters that contain higher and lower
 498 anomaly scores. We define the reward value $R_{\chi,i}$ for snapshot i
 499 as the silhouette score from the dataset clusters that represents
 500 a measure of cluster similarity.

501 Figure 4 shows a high-level illustration of the reinforce-
 502 ment learning role. During real-time operation, 1) the cur-
 503 rent anomaly model's configured detection threshold classifies

ALGORITHM 1: Algorithm for IDS RL Reward

Input : Anomaly scores produced by χ for each window in dataset i ($a_{t,\chi}$)

Output: MAB reward value $R_{\chi,i}$

1 **Function** MABReward:

2 **for** $t \in [1, T]$ **do**

3 $\vec{A}_\chi \leftarrow a_{t,\chi}$;

4 **end**

5 $k = 2$;

6 $\vec{C}_\chi = \text{KMeans}(\vec{A}_\chi, k)$;

7 $R_{\chi,i} = \text{Silhouette}(\vec{C}_\chi)$;

8 **return** $R_{\chi,i}$;

9 **End Function**

504 MDS samples during each monitoring window t . Depending
505 on either the number of samples collected or the time delta
506 between collection periods, 2) MDS sample snapshots (e.g.,
507 M samples across K feeds) are sent to a ‘‘MAB RL’’ function
508 to determine anomaly model hyperparameter χ based on
509 the newly updated data sample of recent and historic MDS
510 samples. Once the updated MDS samples are processed by the
511 ‘‘MAB RL’’ function, 3) the model configuration computed by
512 the RL process is issued as an updated model configuration
513 (χ) for real-time anomaly detection. This process enables the
514 anomaly model configuration to adapt its detection threshold
515 via the RL process to respond to changes in the MDS data
516 sample distribution and to discover previously unidentified
517 threats.

518 Figure 5 shows the reinforcement learning process.

519 • **Real-time detection.** During each detection window t ,
520 following collection and transcription processing (1.1), the
521 presence inference layer classifies the aMDS sample to
522 determine the presence inference state (1.2) and then selects
523 the most appropriate anomaly detection model to use for
524 each subsequent MDS sample forwarded in the window
525 (1.3). The user’s risk threshold θ is used to compute the
526 window’s aggregated anomaly score by means of formula
527 (1).

528 • **Continuous RL adaptation.** Once the sample input thresh-
529 old (which is defined by the sample data size or time delta)
530 is met, the received MDS samples are stored as a snapshot
531 consisting of n windows in the MDS datastore set $[J]$ (2.1).
532 MDS samples are selected at random during each MAB
533 arm iteration. During each trial (2.2), each MDS model is
534 trained with contamination hyperparameter χ (i.e., the MAB
535 action-state parameter), with the MDS dataset excluding the
536 randomly selected MDS snapshot i (i.e., the non-stationary
537 bandit environment). Snapshot i is then used as test data for
538 the trained anomaly model, producing an array of anomaly
539 scores for each window in the snapshot, where the reward
540 $R_{\chi,i}$ is computed by the reward Algorithm 1. Once the
541 number of predefined RL trials has been reached, the χ
542 hyperparameter ‘‘tuned’’ model is selected for use in the
543 real-time anomaly detection process. The RL process is re-

initiated once a new snapshot is stored.

To estimate the reliability of MAGPIE’s reward mechanism,
in section V, we experimentally evaluate two popular MAB
algorithms that are commonly applied in non-stationary and
adversarial bandit problems against a random selection method
and compare their the cumulative average regret, cumulative
average reward and average regret. We then proceed to estab-
lish the quality of the arm (χ) selection for the optimal bandit
method using a fixed step horizon and evaluate the selection by
generating an AUC-ROC model score for the corresponding
isolation forest anomaly classifier configurations.

Monitor state and source detection - The state and source
variables are intended to inform the household of whether the
smart home is subject to anomalous behaviour after computing
the detection score (e.g., under attack), as well as the MDS
feeds with the highest anomaly score, which is indicative of
the utilised attack vector (e.g., IP network, Zigbee network).

3) *Human presence inference:* Certain smart home system
activity is observed irrespective of occupant presence. For
example, a voice-controlled home assistant sends a continuous
keep alive IP packet to the cloud regardless of whether
occupants are using it. Other cases of system activity would be
unusual if no human is present. For example, consider the case
where network traffic from a ZigBee motion sensor increases
dramatically or a voice command is activated even though no
one is home. Therefore, it may make sense to train different
machine learning models for the two cases of presence and no
presence. Human presence inference can be based on a simple
manual process, where occupants set it manually when they go
to sleep or leave home, or it can be performed automatically
before anomaly detection to select the machine learning model
that corresponds to the presence state identified.

IV. PROTOTYPE IMPLEMENTATION AND SETUP

We have evaluated our prototype implementation by inte-
grating it within the smart home of a real household with
three members. Figure 6 shows the layout of the devices,
which are described in Table IV, referenced by number ID
in Figure 6, and accompanied by the smart home automation
rules specified by the household, which are summarised in
Table V. The setup includes a common home Internet router
(2) with a WiFi LAN for WiFi-enabled devices (3-7, 13) and
a ZigBee gateway (8) for Zigbee devices (9-12) connected to
the home router via Ethernet. Remote connectivity to WiFi and
ZigBee devices is facilitated by respective cloud services via
the Internet. MAGPIE (1) collects all local and Internet traffic
traversing the home router via an Ethernet SPAN port. Its WiFi
and ZigBee interfaces passively monitor WiFi and Zigbee
network frames on their configured RF channels. The software
defined radio (SDR) interface captures spectrum readings in
the respective WiFi and ZigBee 2.4 GHz ranges. MAGPIE’s
microphone is directly connected via USB. An adversary
within wireless range of the smart home can execute ZigBee
and WiFi attacks using an attack laptop, SDR peripherals and
ZigBee antennas with customised firmware. The adversary can
also target the smart home remotely via compromised cloud
services or via command and control of compromised devices.
See Table IX for a list and descriptions of the attacks.

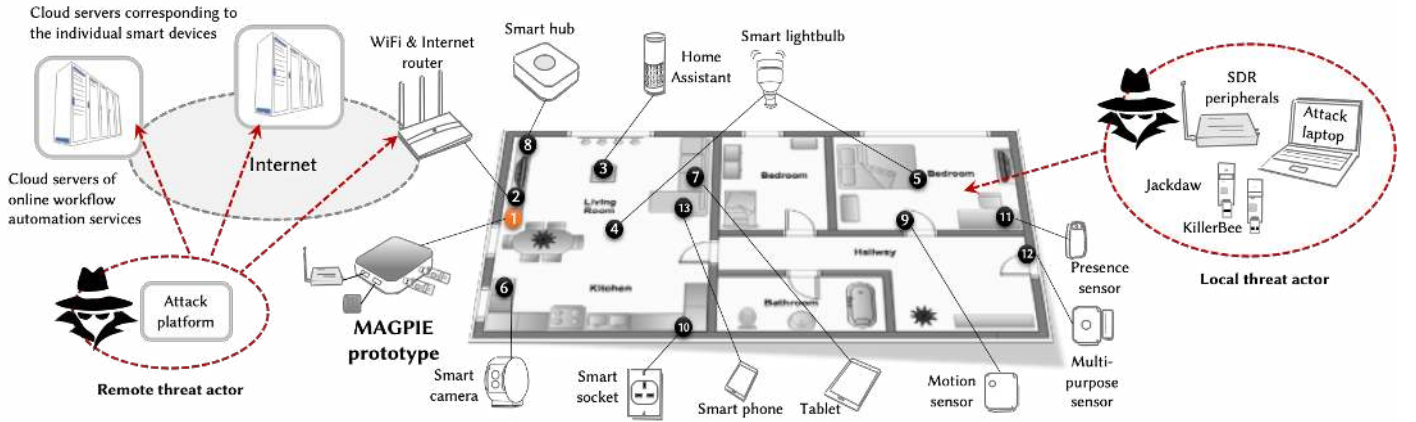


Figure 6: Smart home testbed for MAGPIE prototype experiments

Table III: Live capture sample dataset statistics

Dataset	Mean length	Attack States*	Stdev
45 x Normal	713.7 s	N/A	N/A
10 x A1	36.4 s	.524	0.007
10 x A2	39 s	.542	0.051
10 x A3	25.2 s	.527	0.038
10 x A4	37.8 s	.526	0.018
10 x A5	27.6 s	.572	0.033
10 x A6	25.6 s	.551	0.054
10 x A7	29.2 s	.615	0.283

* Average ratio of attack to normal states during attacks

Figure 7 presents the MAGPIE prototype’s technical schematic. Each MAGPIE interface (1: Ethernet, 2: ZigBee antenna, 3: WiFi antenna, 4: Microphone, 5: SDR RF scanner) has individual data collection and parser processes managed by a window synchronisation daemon to forward all MDS datastreams to a message queue (ZMQ publisher) based on a defined time window. The ZMQ message queue forwards each MDS datastream to a datastore. Then, MDS pre-processing subscribers pull each MDS datastream from the ZMQ message queue, preprocess and forward the prepared MDS feature vectors to each respective MDS Isolation Forest model for anomaly detection and aggregated threat detection output. In parallel, the aMDS feed is forwarded to the random forest presence classifier for presence model selection. MAB RL adapted isolation forest models are trained, stored in the datastore and then loaded into the anomaly model selection and detection process after every MAB RL iteration.

The behaviour of occupants in the testbed and their interactions with the smart home devices and automation rules was allowed to occur naturally, with the addition of some requested actions to ensure that all automation rules or devices were activated during data collection. Training data collection was conducted intermittently during a 1-month period. The locations of the MAGPIE prototype and IoT devices remained static, with the exception of the mobile and tablet devices, which moved with the occupants using them. In total, there were 45 normal data collection runs with an average length of 713.7 s each and 70 attack data collection runs with an average length of 31.5 s each. In Table III, we provide summary statistics related to the datasets collected during the 1-month experiment.

A. Cyber-physical meta-data features in the smart home

In Table VI, we present each of the cyber-physical MDS feeds and the corresponding features collected. Further statistical flow information, such as sample frequency, average and standard deviation metrics, are added during parsing. We utilise tshark’s display filter at run-time for standard input into the MDS parser, applying only regex operations to input data. Note that for physical data sources such as audio and radio frequency spectrum, we utilise custom (a python application) and open-source libraries (rx_power from rx_tools [34]) for feature collection. On the testbed, we apply the following constraints based on observation:

- WiFi data frames are redundant and ignored as they provide the network footprint, which is already monitored in encapsulated IP packets. WiFi “Request/Clear to Send” control frames are ignored as these are mainly used to avoid hidden-node collisions. Therefore, only WiFi management frames, which can be exploited to disrupt or infiltrate a WiFi network, are monitored.
- ZigBee sensors and actuators, with the exception of coordinator nodes (e.g., gateways), use dynamic network addressing. Therefore, all non-coordinator nodes are addressed using the same numerical value. This does not impact the ability to model anomalous ZigBee patterns as sensor and actuators generate a fairly predictable network footprint.
- Radio frequency spectrum analysis covers the 2.4 GHz frequency band for 802.11G and ZigBee, which can also include Bluetooth and other 802.15.4 wireless protocols.

1) Risk-based unsupervised threat monitoring with reinforcement learning adaptation:

- **Isolation forest anomaly detection.** We have opted to implement unsupervised anomaly detection using the isolation forest algorithm in Python with the Scikit Learn library [35]. It performs anomaly detection by isolating sample data points through random feature selection and value splitting, selecting a random value between the maximum and minimum bounds of a data sample feature. No prior assumptions are made regarding the distribution of feature values. Therefore, randomised feature splitting is effective for hybrid feature-sets of both continuous and categorical

Table IV: Smart home testbed devices and network connectivity

ID	Device Type	Interface	Description
1	MAGPIE prototype	ZigBee, WiFi, RF, Audio, Ethernet (IP)	Raspberry PI 3 "MAGPIE-enabled" prototype
2	WiFi router	WiFi 802.11G, Ethernet (IP)	Vodafone Broadband home router
3	Home assistant	WiFi (IP)	Amazon Echo voice-controlled home assistant connected to WiFi router
4, 5	Smart lightbulb	WiFi	LIFX smart light bulb connected to WiFi router & Amazon Echo via Cloud
6	Smart camera	WiFi (IP)	Somfy Protect smart camera connected to WiFi router & IFTTT via Cloud
7	Tablet	WiFi	Samsung S2 tablet connected to WiFi router
8	Smart hub	Ethernet (IP), ZigBee, Zwave	SmartThings hub connected nodes via ZigBee & WiFi router via Ethernet (IP)
9	Motion sensor	ZigBee	SmartThings motion sensor connected to smart hub via ZigBee
10	Smart outlet	ZigBee	SmartThings power outlet connected to smart hub via ZigBee & Amazon Echo via Cloud
11	Presence	ZigBee	SmartThings presence sensor key chain dongle connected to smart hub via ZigBee
12	Multi-purpose sensor	ZigBee	SmartThings multi-purpose sensor connected to smart hub via ZigBee
13	Smart phone	WiFi, Cellular (3/4G)	Connected to WiFi router (external connectivity to smart home control software via 3/4G)

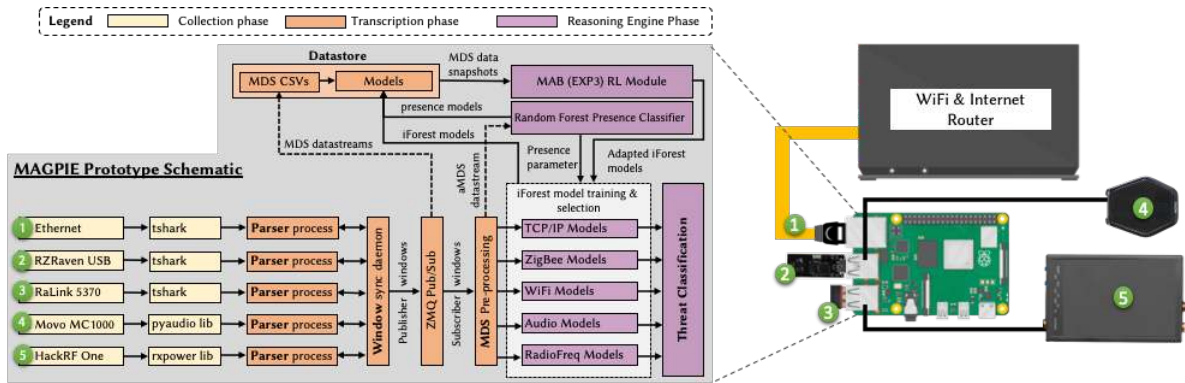


Figure 7: MAGPIE prototype technical schematic

Table V: Smart Home testbed automation integration and rules

Trigger Platform	Action	WAS	Antecedent
Amazon Echo	Voice trigger command	IFTTT	Somfy Protect actuation
Amazon Echo	Voice trigger command	Alexa Skills	LIFX bulb actuation
Amazon Echo	Voice trigger command	Alexa Skills	Outlet actuation
SmartThings	Mobile app "On" button	SmartThings	Outlet actuation
SmartThings	Door-open detection	SmartThings	SmartThings Multi-sensor
Amazon Echo	Motion sensor detection	IFTTT	Somfy Protect Arm/Disarm
LIFX	Mobile app "Bulb" button	LIFX	LIFX bulb actuation

WAS: Workflow Automation Service

Table VI: MAGPIE prototype data feeds and meta-data stream (MDS) features

Data feed	Input	Base Features
IPv4 (TCP/IP) pkts	C	src*, dest*, port, pkt type, pkt sz, ttl*, pkt delay, flow dir*
WiFi 802.11 frames	C+P	src*, dest*, port, frame type, frame sz, rssi, frame delay
ZigBee (802.15.4) pkts	C	src*, dest*, pkt type, pkt sz, pkt delay
Microphone audio	P	rms frequency threshold, rms
RF (2.4GHz) Spectrum	P	† dB power level (per frequency bin)

C = Cyber, P = Physical, *aMDS: not used, † aMDS: Avg/Stdev of all bins

672 data, as is the case with MDS feeds. The recursive feature
 673 partitioning represents a tree structure, whereby the number
 674 of times a feature is split to isolate a sample follows a
 675 traditional tree path length from the root to a terminating
 676 node. The average tree path length represents the decision
 677 function used to classify observations as normal or anomalous
 678 [26]. For each MDS feed generated, an independent
 679 feed-specific isolation forest model is created. Together, the

680 forests form an ensemble of models used to produce an
 681 aggregate anomaly score during each monitoring window.

- 682 • **Adversarial multi-armed bandit reinforcement learning.**
 683 MAGPIE models threat detection adaptation in a smart
 684 home as an adversarial bandit environment based on the
 685 premise that what is normal behaviour (e.g., devices, net-
 686 work traffic, user interaction) may frequently change in
 687 a smart home. Therefore, MAGPIE trains its RL-based
 688 anomaly classifiers on a continuously changing series of
 689 collected dataset snapshots. At each time step, for each
 690 arm pull (i.e., isolation forest χ hyperparameter selection),
 691 the smart home bandit chooses at random a dataset to test.
 692 Therefore, on the basis of algorithm 1, the distribution of
 693 reward $R_{\chi,i}$ for each action state arm is drawn from an
 694 i.i.d. distribution based on randomly selected MDS dataset
 695 snapshots. In this case, as each arm's reward distribution
 696 changes at random in the adversarial bandit environment,
 697 the EXP3 (exponential-weight algorithm for exploration and
 698 exploitation [33, 36]) algorithm is a natural and suitable
 699 choice to establish the optimal χ configuration for the
 700 isolation forest. For comparison against EXP3, we also
 701 select a non-stationary sliding-window based UCB (upper-
 702 confidence bound) algorithm [37], where the reward policy
 703 is weighted according to a constant step size used to update
 704 the reward estimate (we defined a step size of 0.1, which
 705 moves the agents estimate 10% closer to the most recent
 706 observed reward). UCB is a popular choice for traditional
 707 stationary MAB reinforcement learning problems, achieving

MAB Algorithm	Parameters
EXP3	$\gamma = 0.1$, arms* = 10, iters.†=6000
Non-stationary UCB1	exploration (C) = 2, $\lambda = 0.1$, arms* = 10, iters.†=6000

*hyperparameter configurations, † action-step horizon

Table VII: EXP3 and non-stationary UCB1 MAB parameters

Table VIII: MAGPIE prototype *Reasoning Engine* model configuration parameters

Anomaly detection (Unsupervised learning) configuration	
Algorithm	Isolation Forest
Trees (C)	200 (per MDS model)
Sub-sampling (ψ)	250 (per MDS model)
Bootstrap	Sampling without replacement
Max Features	All features (randomly selected per split)
Contamination (χ)	Bins = 0.001, 0.002, 0.005, 0.01, 0.2, 0.05, 0.1, 0.2, 0.5, 0.7
θ	0.1, 0.3, 0.5, 0.7, 0.9
Presence inference (Supervised learning)	
Algorithm	Random Forest
Trees (C)	100
Sub-sampling (ψ)	250 (per MDS model)
Max Depth	15
Bootstrap	Sampling without replacement
Max Features	Auto (max features= $\sqrt{\text{features}}$)
θ	0.3, 0.5, 0.7
Detection adaptation (Reinforcement learning) configuration	
Algorithm	EXP3 ($\gamma=0.1$, 6000 step-horizon)
Reward metric	As per section III-A
Presence	1 (Activity), 0 (No activity)
MAB Arms	10 - (Contamination χ Bins)

708 logarithmic regret for the number of actions/arm pulls (in
709 this case, χ parameters) selected over time [38], where
710 regret refers to the expected decrease in reward gained
711 during execution of the learning algorithm instead of acting
712 optimally [39]. In other words, the regret is the difference
713 between the reward of a given policy (i.e., the learning
714 algorithm) and that of the optimal static policy in hindsight.
715 In this case, to adjust to stochastic, non-stationary bandit
716 behaviour, a discounting factor (λ) based on a step-size
717 sliding window is applied to a UCB1 policy reward estimate.
718 The EXP3 and non-stationary UCB1 implementations were
719 adapted from the bandit algorithms developed in [40] and
720 [41], respectively. In Table VII, we summarise the config-
721 uration parameters for the EXP3 and non-stationary UCB1
722 algorithms.

723 2) *Human presence inference*: In our implementation, the
724 presence of people is detected with a supervised random forest
725 (RF) classifier using ground-truth labels defined by the user,
726 as RF is commonly used for lightweight machine learning in
727 the IoT [42]. Other lightweight supervised machine learning
728 classifiers are similarly useful. Labelling of aMDS data sam-
729 ples (user presence (1)/no user presence (0)) is pre-configured
730 for the initial training of the prototype during the start-up
731 learning phase. Subsequent training requires users to actively
732 inform MAGPIE of the time periods in which they are actively
733 present in the household (unsupervised presence inference is
734 outside the scope of the prototype development). We define a
735 simplified household environment for presence inference based
736 on whether occupants are actively or passively interacting with
737 the smart home network. By observing the behaviour of a sub-

sample of collected aMDS data points (Figure 8), we see a
738 distinguishable impact of presence and no presence for most
739 datastreams. However, aside from other physical sources, basic
740 sound measurements as a feature may be problematic in the
741 face of an audio injection attack. We evaluate this impact
742 on automated presence inference in section V-A, where we
743 also assess overall detection results, showing that presence
744 inference helps increase accuracy.
745

B. Smart home cyber-physical attack vectors

746 We have subjected our testbed to attacks targeting WiFi,
747 ZigBee and voice-enabled home assistant communication tech-
748 nologies, as well as corresponding smart home device control
749 software and third-party apps, all of which are commonly
750 deployed within today’s smart home environments. WiFi is
751 currently the primary connectivity medium in most smart
752 homes, not only for device-to-device communication but also
753 as a network gateway to the cloud services on which most
754 smart home devices rely. ZigBee is a low-powered wireless
755 medium that provides energy-efficient connectivity for low-
756 resource devices that connect to more capable control gate-
757 ways (e.g., ZigBee hub with Ethernet or WiFi backhaul). How-
758 ever, it has limited bandwidth for data communication (250
759 kbit/s per channel in the 2.4 GHz band used in the testbed).
760 Security-wise, the speaker-microphone pair of a voice-enabled
761 home assistant is typically an unmonitored communication
762 link, which has been shown to be vulnerable to exploitation
763 [44]. Smart home devices such as security cameras offer
764 physical monitoring protection of the household; however,
765 recent high-profile compromises of these types of systems have
766 demonstrated how their exploitation can lead to significant
767 breaches of the physical privacy of occupants and, in some
768 cases, impact their emotional well-being [6].
769

770 In Table IX, we describe the attack vectors and their cyber-
771 physical impact based on [5]. All attacks were executed in both
772 the presence and no presence conditions. Note that localised
773 attack vectors (namely, WiFi death (A1), Evil twin (A2),
774 ZigBee jamming (A3) and Node amplification (A4)) could also
775 be launched remotely if a target device were compromised
776 through third-party apps, cloud-based control software, or
777 compromised software and hardware supply chains [6]. For
778 example, both home assistants and smart lightbulbs provide
779 the ability to host their own WiFi access point, whilst ZigBee
780 devices are capable of reconfiguring themselves as ZigBee
781 network coordinators.

C. Experimental scenario, settings and parameters

782 Our experimental process consisted of three phases. Phase
783 1 was related to (i) live sample data collection of smart home
784 behaviour (in terms of the data sources monitored) when not
785 under attack and (ii) execution of each attack vector. This
786 phase comprised two different types of experiments: one where
787 users were present during data collection and another where
788 no users were present in the household. Phase 2 was related to
789 the adaptation of the offline reinforcement learning anomaly
790 detection. Phase 3 was related to live monitoring of attack
791 detection using the RL-optimised MAGPIE configuration.
792

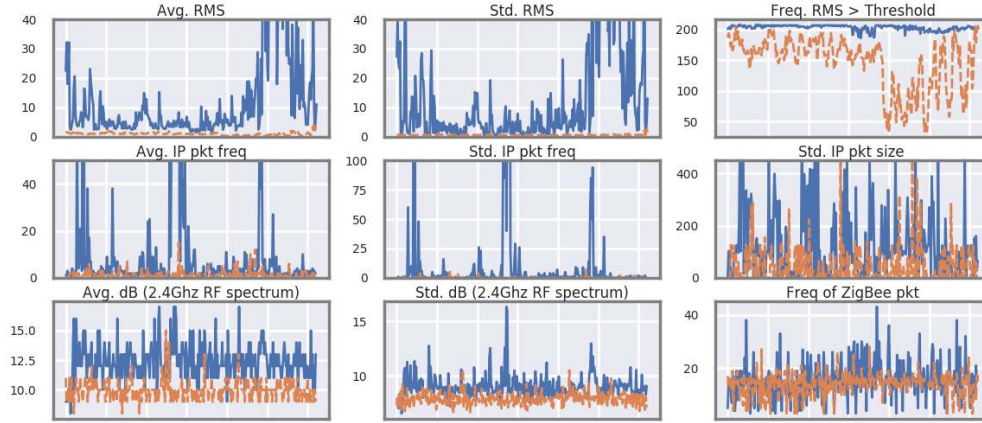


Figure 8: Aggregated MDS (aMDS) behaviour during “No presence” (orange dashed line) and “Presence” (blue line) states.

Table IX: Experiment attack vectors with cyber-physical impact classification [6] in the smart home

Attack*	Layer	C*	P*	Description
(A1) WiFi deauth	Data Link	A	PA, DA	WiFi deauthentication frame flood, resulting in prevented or delayed actuation and DoS for all WiFi hosts. Executed with <i>aircrack-ng</i> suite.
(A2) WiFi Evil Twin	Data Link	C, I, A	PA, IA	Evil twin (ET) spoofs WiFi network disrupting WiFi-connected devices; entices connection to attacker-controlled access point. Results in prevented actuation through WiFi beacon frame interference and incorrect actuation for ET-connected devices under the control of the attacker. Executed using the <i>aircrack-ng</i> suite.
(A3) ZigBee jamming	Physical	A	PA	ZigBee communication is jammed on current radio frequency. Results in prevented or delayed actuation . Executed with the RZRAVEN USB Stick flashed with Jackdaw firmware [43].
(A4) ZigBee node amplification	Network	I, A	DA	Targets a vulnerability in <i>Samsung SmartThings</i> smart outlet, which acts as a router/relay in the ZigBee PAN. An unsolicited ZigBee data request sent to the <i>SmartThings outlet</i> returns four encrypted data packets in response. Replay of a doctored PCAP containing a large volume of data requests triggers exponential traffic amplification against the outlet. The resulting volume of data packets returned quickly overwhelms the <i>SmartThings</i> network bandwidth resulting in prevented or delayed actuation . Executed using the RZRAVEN USB Stick with KillerBee suite https://github.com/riverloopsec/killerbee . After our ethical disclosure to the manufacturer, the vulnerability has since been patched.
(A5) Malware audio injection	Physical & Application	I	UA	Compromised smart device (Samsung Tablet) with its on speaker-microphone pair injects malicious commands into the <i>Amazon Echo</i> home assistant, eliciting unauthorised actuation . The commands continuously arm or disarm the smart camera and turn on or off any household lights. A second-order impact is the DoS of smart home systems that may also be used to detect physical intrusion. A remote command and control channel directs the execution of the audio injection. Executed using <i>Stringify</i> API as the command and control channel to a custom Android app that plays and records audio (for audio-based camera actuation).
(A6) Security camera compromise	Application	C	UA, BP	Compromised smart home security camera user credentials (e.g., phishing/insecure network) used to create a remote connection to the camera video feed (breaching physical privacy). Executed using the user credentials to obtain an authentication token issued by the <i>Somfy Protect</i> API.
(A7) Workflow automation compromise	Application	C	UA, BP	Compromised smart home IFTTT user credentials (e.g., phishing or insecure network). Issues actuation commands via occupant workflow automation rules (“Arm/Disarm camera”, “Turn on light bulb”, etc.), disrupting smart home devices via unauthorised actuation . Smart outlet, camera and bulbs are continuously issued actuation commands at high frequency; light bulb set to “flicker”, which could lead to medical impact in the form of seizures for occupants with photosensitive epilepsy or to electrical damage caused by surges in voltage.

*See attack cyber-physical impact graphs: <https://github.com/isec-greenwich/magpie>

C* (Cyber impact)- C: Confidentiality, I: Integrity, A: Availability

P* (Physical impact)- PA: Prevented Actuation, IA: Incorrect Actuation, UA: Unauthorised Actuation, DA: Delayed Actuation

BP: Breach of physical privacy

793 Table III provides statistics about the live capture sample
 794 dataset for normal and attack execution experiments. Some
 795 attack vectors (WiFi de-authentication and ZigBee jamming)
 796 were observed to have a persistent effect on specific device
 797 behaviour, such as total connectivity loss to the WiFi network
 798 or disconnection of ZigBee nodes from the PAN, even after
 799 the attack had stopped. To ensure that persistent symptoms of
 800 one experiment did not interfere with another, after each attack
 801 execution, we reconnected affected devices and nodes to their
 802 respective networks and tested the automation rules to ensure
 803 that the smart home had returned to a known good state. For
 804 phase 1, each attack vector was executed independently so
 805 that normal and attack data samples were equally distributed

with respect to the amount of time the smart home was
 monitored by MAGPIE under normal conditions and during
 attack execution. This process ensured that the captured dataset
 had a balanced set of normal and attack samples for testing.
 All live sample collection experiments were conducted on the
 training data for phase 2 reinforcement learning adaptation of
 the MAPGIE’s anomaly models, whereas phase 3 consisted of
 executing live attack vectors against the MAGPIE prototype in
 a real-time monitoring state with the optimised anomaly model
 configuration. During the experiment, the users interacted with
 the smart home according to their normal routine. This activity
 generated a dataset that represented natural smart home user
 behaviour. Table X shows the different types of interactions

806
807
808
809
810
811
812
813
814
815
816
817
818

Table X: Summary of occupant device and network interaction in the smart home testbed

Device / Platform	Action	Activity description
SmartThings Multi-Sensor	P, T, S	Opening/closing door & status check on app
SmartThings Motion-Sensor	P, T, S	Moving in range of motion sensor & status check on app
Smart Outlet	P, T, S	Turning on/off via button & app & status check on app
Amazon Echo (via Voice)	P	Asking questions, playing music, triggering LiFX, Somfy
Amazon Echo (via app)	P, T, S	Playing music, Amazon Echo activity & changing Alexa skills
Somfy Protect	P, T, S	Reviewing camera feed, triggering security mode via Somfy app
LiFX lightbulbs	P, T, S	Triggering LiFX bulbs via the LiFX mobile app

*P=Physical, T=Tablet, S=Smart phone

819 performed by the users.

820

V. EXPERIMENTAL RESULTS

821 The MAGPIE prototype’s performance is evaluated in terms
822 of the i) attack detection accuracy with reinforcement learning
823 χ adaptation Vs. random χ configuration, and the effect on
824 performance with and without cyber-physical sources of data;
825 ii) accurate detection of presence in the smart home and its
826 effect on threat detection performance for dynamic anomaly
827 model selection; iii) attack detection latency, which refers to
828 the time delay before the prototype system correctly identify
829 an attack, taking into account correct interface *source detec-*
830 *tion*; and iv) end-to-end monitoring latency, which measures
831 the processing delay for each of the MAGPIE prototype’s
832 *transcription* and *analysis* phases to complete, according to
833 the prescribed collection window interval.

834 For each measure of detection performance, we employ
835 timestamp window labelling to indicate whether a predicted
836 data sample’s label belongs to an attack window or a non-
837 attack window. In terms of accuracy, the Jaccard similarity
838 coefficient is used as a measure of prediction performance to
839 compare a set of predicted data sample labels to a correspond-
840 ing set of ground truth labels.

A. (Contribution 1) Ability to recognise new smart home threats by continuous adaptation to changing conditions

843 At its inception, a newly installed smart home can be
844 safely assumed to be free from attacks. Therefore, a low
845 anomaly detection sensitivity (e.g., χ - contamination value
846 for isolation forest anomaly decision function) is a sensible
847 choice for system initialisation. However, over time, the level
848 of data contamination supporting this condition will drift due
849 to changes in the smart home configuration or actual attacks
850 (which may be undetectable at the time of occurrence due to
851 the current detection sensitivity). The same applies to selecting
852 the anomaly detection sensitivity for an existing smart home.

853 In Figures 11 and 10, the experimental results of the RL
854 training show that EXP3 achieved the lowest average cumu-
855 lative regret and highest average cumulative reward compared
856 to a non-stationary UCB strategy, whereas both EXP3 and
857 UCB comfortably outperformed a naive random arm selec-
858 tion strategy. In terms of cumulative reward, initially, minor
859 increases in observed reward occur due to the relatively small
860 distribution range between rewards (see Figure 10). The effect
861 on performance for both EXP3 and UCB therefore indicates
862 that a sufficiently large step horizon is required to reach an
863 optimal and reliable arm selection state, as per the objectives of
864 the MAGPIE MAB RL process. Following our experimental
865 comparison of MAB algorithms, EXP3 was selected as the

P*	θ	χ Mode*	ACC	TPR	TNR	PPV	NIR
✓	0.3	Random† RL	0.67 0.85	0.78 0.99	0.55 0.82	0.66 0.64	0.60 0.60
✗	0.1	Random† RL	0.68 0.87	0.79 0.90	0.56 0.87	0.68 0.83	0.61 0.61

Table XI: Average detection accuracy for RL χ adaptation Vs. randomly selected χ , P* Occupant presence in smart home testbed, † Average over 100 runs, selecting from 10 bandit Arms (i.e., χ bins - see Table VIII)

866 optimal bandit algorithm for solving the anomaly classifier
867 detection adaptation objective in MAGPIE. Following a fixed-
868 step horizon selection policy, in Figure 12, EXP3 reported
869 optimal arm weights $\chi=0.01$ (ARM 4) and $\chi=0.005$ (ARM
870 3) for the presence and non-presence anomaly classifier con-
871 figurations, respectively. To analyse the quality of the EXP3
872 selected χ configuration parameters, we derived AUC-ROC
873 curves for models trained with each specific χ parameter in
874 Figure 13. The results show that for overall model detection
875 accuracy, when applying the θ threshold across all attacks
876 we evaluated, EXP3 selected the optimal χ parameter for the
877 presence and no-presence anomaly models. In terms of overall
878 AUC, the selected arms were ranked first (AUC=0.90) and
879 third (AUC=0.88) for the presence and no-presence models,
880 respectively.

881 In summary, the results presented in Table XI demonstrate
882 that the combination of EXP3 with our probabilistic reward
883 algorithm is a reliable mechanism for optimising detection
884 performance. Figure 9 shows RL optimised the unsupervised
885 detection accuracy for each θ when tested against the attack
886 vector in our testbed.

887 Analysis of the presence datasets (orange radar) shows
888 poor detection accuracy for attack A5 (malware-enabled audio
889 injection; ACC: 60% Vs. 55% no information rate - NIR). This
890 decrease in accuracy when occupants are present is likely due
891 to the attack pattern of A5 blending in with the occupants’
892 own use of the home assistant. Therefore, to improve detection
893 of A5 in future work, more expressive features are required
894 (such as voice command recognition or individual modelling
895 of sound and IP/WiFi traffic mean absolute deviation according
896 to the time of day) to provide greater behavioural context
897 to the anomaly detection process. Omitting A5 from the
898 aggregated results yields an overall detection accuracy for
899 occupant presence models of 89%, an F1 score of 81%, TPR
900 of 99%, TNR of 84% and precision of 72%. On the other hand,
901 A5 is easily detectable by no-presence models (for the static
902 presence model configuration) due to the abnormal occurrence
903 of sustained levels of sound, with a detection accuracy of 93%.
904 The no-presence model achieved an F1 score of 85%, TPR of
905 90%, TNR of 87% and precision of 83%. For individual attack
906 adaptation, RL also reports fairly low accuracy for attack A7
907 in the presence models and attack A6 in both the presence and
908 no-presence models.

909 In practice, the optimal θ for presence and no-presence
910 threat detection may not be selected as the preferred value.
911 Importantly, the results show that a range of different θ settings
912 influence the RL adaptation process, whereby high θ values

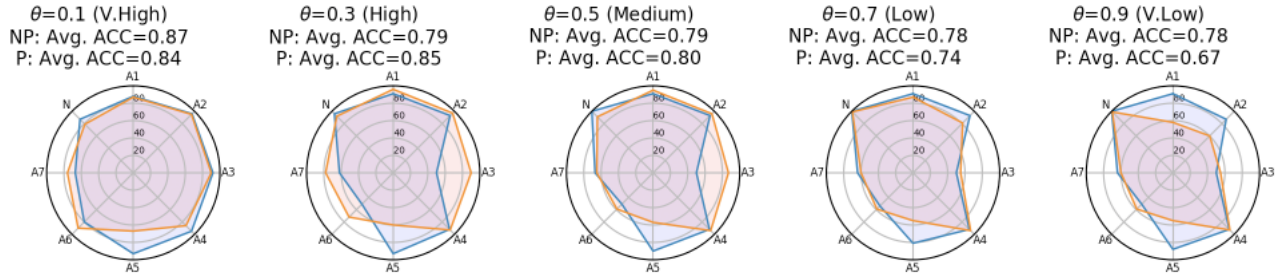


Figure 9: Risk-based RL-optimised anomaly detection accuracy [%] (Presence = Orange, No Presence = Blue, MAB Arm 3: $\chi = 0.005$, MAB Arm 4: $\chi = 0.01$)

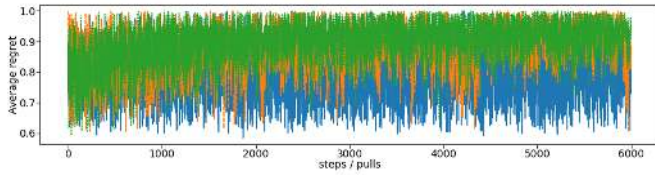
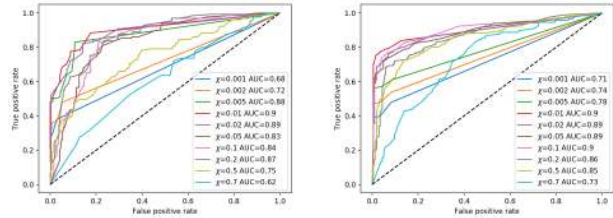
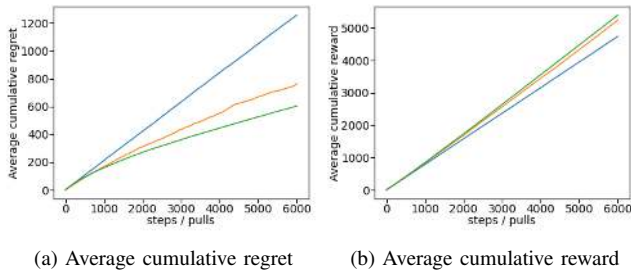


Figure 10: Average cumulative χ selection regret for random (blue), non-stationary UCB (orange dash), and EXP3 (green points) MAB algorithms over a 6000 step horizon across 3 runs



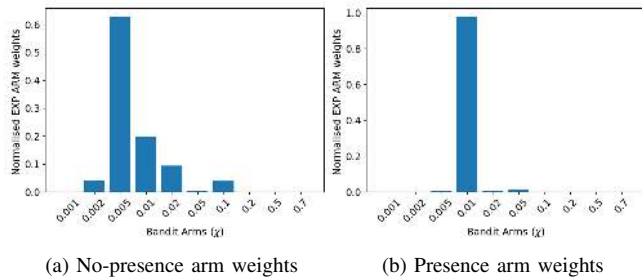
(a) No-presence AUC ROC (b) Presence AUC ROC

Figure 13: AUC ROC curves for MAGPIE bandit arms (χ hyperparameters)



(a) Average cumulative regret (b) Average cumulative reward

Figure 11: Cumulative χ selection reward and regret for random (blue), non-stationary UCB (orange) and EXP3 (green) MAB algorithms over a 6000 step horizon across 3 runs



(a) No-presence arm weights (b) Presence arm weights

Figure 12: EXP3 weights for bandit arms (χ) over a 6000 step horizon

(0.7 and 0.9) are the least effective for both presence and no-presence models. In general, high θ favours high anomaly scores, which reduces false positives but may increase false negatives. This characteristic can be observed for attack A7 (workflow automation compromise), where MAGPIE reduces each set of attack data points to a single sample per window (based on source and destination identity), which in turn is saturated by a high volume of normal traffic, thus lowering the anomaly score. Overall, the detection results illustrated in Figure 9 demonstrate that the non-stationary UCB implementation is effective at adapting the detection sensitivity to optimise the threat detection performance according to the occupants' θ configuration. From here on, we assess the MAGPIE prototype's threat detection performance according to the best-performing θ and RL optimised isolation forest χ parameters.

B. (Contribution 2) Considering both cyber and physical sources of data

Applying the best θ and χ parameters, for both individual and aggregate attack dataset RL adaptation, in Figure 14 the detection accuracy for the presence and no-presence models across different MDS cyber and cyber-physical feature models is presented. Here, MAGPIE prototype threat detection is demonstrably more accurate, on average, when both cyber and physical smart home data sources are used compared to cyber features only. However, even without physical features (in this case RF, audio and WiFi RSSI), extending the collection of cyber features beyond traditional monitoring of TCP/IP traffic significantly improves the detection accuracy across a wide range of attack vectors in the smart home.

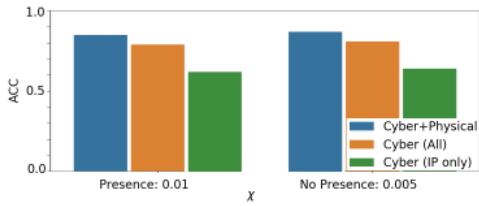


Figure 14: Attack detection performance results comparison for MDS models with cyber+physical features, multiple cyber features and cyber features based on the TCP/IP stack only

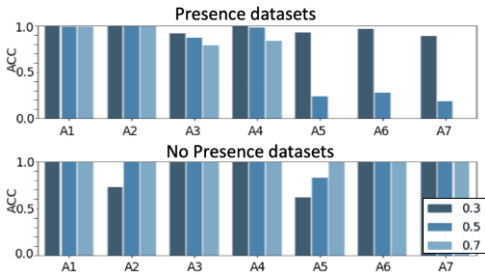


Figure 15: Presence inference accuracy for each attack (Avg. ACC: $\theta = 0.3=0.93$, $\theta = 0.5=0.81$, $\theta = 0.7=0.76$)

943 **C. (Contribution 3) Self-configuration based on automated**
 944 **inference of human presence**

945 Figure 15 shows that presence inference returned high clas-
 946 sification accuracy during both attack and non-attack scenar-
 947 ios. A choice of $\theta = 0.3$ yielded the highest overall accuracy
 948 (93%) across both the presence and no-presence datasets.
 949 However, there is a noticeable accuracy drop compared to
 950 static detection model assignment for correctly detecting pres-
 951 ence during the audio injection attack (A5) when there is no
 952 presence (62%). This is because the random forest detection
 953 model has determined higher audio values to be associated
 954 with presence state and thus incorrectly identifies the audio in-
 955 jection attack as occupant presence. Consequently, this failure
 956 has a negative impact on the detection of audio injection with
 957 a high sensitivity for presence inference. On the other hand,
 958 whilst increasing θ to 0.5 increases the detection accuracy for
 959 audio injection during no presence (83%; increasing further
 960 to 97% for $\theta = 0.54$ - not shown in Figure 15), this change
 961 has a negative effect on detection accuracy for attacks A6 and
 962 A7 and further reduces the A5 detection accuracy during the
 963 occupant presence state.

964 Figure 17 shows a noticeable advantage of dynamic recon-
 965 figuration based on presence inference. When utilising the best
 966 high and very high θ values for presence and no-presence
 967 anomaly models, respectively, the method achieves slightly
 968 lower detection accuracy overall (significantly lower in the
 969 case of audio injection - A5 for non-presence) compared to
 970 static model assignment (which requires explicit occupant re-
 971 configuration to function, e.g., the occupant informing the
 972 system when they are no longer present or active). Crucially,
 973 however, without static or dynamic anomaly model assign-
 974 ment, for both the presence and no-presence models, individual
 975 detection performance for alternate datasets is considerably
 976 worse overall.

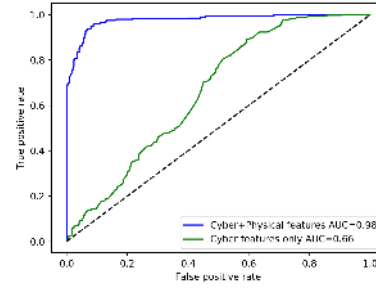


Figure 16: AUC ROC curve (TPR Vs. FPR) performance for presence inference during smart home attacks

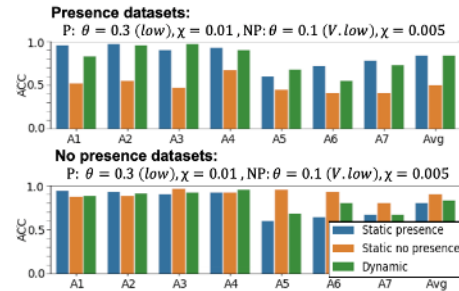


Figure 17: Performance for static presence, no presence and dynamic real-time presence anomaly model selection

977 The experimental results are promising, especially as the
 978 fusion of cyber and physical MDS features has proven to
 979 be valuable for improving presence inference, as further ev-
 980 idenced in the area under curve (AUC) receiver operating
 981 characteristic analysis on new, unseen MDS data shown in
 982 Figure 16. Compared to the AUC score of 0.66 when only
 983 cyber data sources are used, the aggregation of cyber and
 984 physical data sources (i.e., the aMDS feed) yields an AUC of
 985 0.98 for presence inference. Here, instead of training a single
 986 MDS model for both presence and anomaly detection, affected
 987 by increases in model dimensionality and feature-masking for
 988 window synchronisation, these results demonstrate that a ded-
 989 icated presence classifier supports the selection of presence-
 990 specific MDS models that directly benefit from the feature
 991 context to detect attacks more accurately.

992 **D. Threat detection latency**

993 Analysis of the detection latency using the best θ and
 994 χ RL parameters for the presence and no-presence datasets
 995 produced variable results for each attack. These differences
 996 were expected, as the impact of different attacks on cyber
 997 and physical feature behaviour may only become noticeable
 998 later in the course of execution. For attacks A1, A2 and A7,
 999 during human presence, detection was immediately triggered
 1000 (detection latency = 1 monitoring window) when the attack
 1001 was executed in the collection window, but the initial discovery
 1002 of A3 and A4 was three times slower and that of A6 was five
 1003 times slower. In the presence condition, A5 was undetectable.
 1004 In the no human presence condition, attacks A2, A4 and
 1005 A5 reported immediate detection, A1 and A3 required an
 1006 additional collection window for identification, and A6 and

A7 were four and three times slower, respectively. MAGPIE has demonstrated that it is able to detect an attack soon after it is executed, but there remains a trade-off in detection latency and detection accuracy to be explored in the future.

VI. FUTURE WORK

In future work, the q parameter is an interesting and potential candidate for further exploration within the RL action-space for dynamic q assignments, alongside unsupervised model hyperparameter adaptation. However, a consideration when introducing q in this manner is that it increases the computational complexity for the RL action-space. As observed in Figure 3, the benefit of the increased complexity does not clearly outweigh the simpler static q definition. Therefore, dynamic determination of the optimal q is an area that would ideally be explored in the context of collaborative learning, such as federated threat detection adaptation in experiments across multiple coordinating households and MAGPIE agents, with varying MDS configurations and contrasting attack vectors.

It would also be interesting to explore how MAGPIE's detection adaptation might be applied in the form of cyber resilience capability for machine-learning-based intrusion detection itself, for example, as a proactive defence mechanism against emerging adversarial machine learning attacks [45] that disrupt detection accuracy in cyber-physical systems.

VII. CONCLUSION

We have evaluated MAGPIE in terms of four primary contributions: the ability to detect previously unseen attacks while taking into account the user's risk tolerance; the ability to adapt to changing conditions via reinforcement learning; the benefit of using both cyber and physical sources of data; and self-configuration of the choice of models based on whether user presence is detected or not. The prototype has performed well across a range of attack vectors at the application, network, data link and physical layers. We have observed that the incorporation of physical sources of data can noticeably improve the performance for most of the attacks, especially for attacks that are normally undetectable by systems that monitor only TCP/IP traffic. We have also observed that by leveraging the same data sources as for anomaly detection, we can detect user presence sufficiently reliably, which in turn helps tailor the anomaly detection models to the two cases of presence and no presence, thereby improving their accuracy. Most importantly, we have successfully tested our intuition that in the context of smart home attacks, reinforcement learning can meaningfully adapt an unsupervised anomaly classifier's hyperparameters based on its own confidence in its output.

We have made the source code of the MAGPIE implementation available to the research community to facilitate extensions and experimental evaluation comparisons with new methods. A natural extension would be to add real-time response capabilities, such as isolating offending nodes or re-configuring the radio frequency channel. Additionally, MAGPIE can be extended to incorporate feedback from the user, for example, to confirm whether a suspected anomalous device or network behaviour is a result of their own activity or not, to further improve the accuracy.

REFERENCES

- [1] F. Meneghello, M. Calore, D. Zucchetto, M. Polese, and A. Zanella. IoT internet of threats? A survey of practical security vulnerabilities in real IoT devices. *IEEE Internet of Things Journal (early access)*, 2019.
- [2] M. Conti, A. Dehghantanha, K. Franke, and S. Watson. Internet of things security and forensics: Challenges and opportunities, 2018.
- [3] D. Formby and R. Beyah. Temporal execution behavior for host anomaly detection in programmable logic controllers. *IEEE Transactions on Information Forensics and Security*, 15:1455–1469, 2019.
- [4] A. Ameli, A. Hooshyar, A. H. Yazdavar, E. F. El-Saadany, and A. Youssef. Attack detection for load frequency control systems using stochastic unknown input estimators. *IEEE Transactions on Information Forensics and Security*, 13(10):2575–2590, 2018.
- [5] G. Loukas. *Cyber-physical attacks: A growing invisible threat*. Butterworth-Heinemann, 2015.
- [6] R. Heartfield, G. Loukas, S. Budimir, A. Bezemskij, J. R.J. Fontaine, A. Filippoupolitis, and E. Roesch. A taxonomy of cyber-physical threats and impact in the smart home. *Computers & Security*, 78:398–428, 2018.
- [7] M. Alshahrani and I. Traore. Secure mutual authentication and automated access control for IoT smart home using cumulative keyed-hash chain. *Journal of Inf. Security and Applications*, 45:156–175, 2019.
- [8] B. Chifor, I. Bica, V. Patriciu, and F. Pop. A security authorization scheme for smart home Internet of Things devices. *FGCS*, 86:740–749, 2018.
- [9] B. Baruah and S. Dhal. A two-factor authentication scheme against fdm attack in IFTTT based smart home system. *Computers & Security*, 77:21–35, 2018.
- [10] E. Anthi, L. Williams, and P. Burnap. Pulse: An adaptive intrusion detection for the Internet of Things. In *Living in the Internet of Things: Cybersecurity of the IoT*, 2018.
- [11] E. Anthi, L. Williams, M. Sowiska, G. Theodorakopoulos, and P. Burnap. A supervised intrusion detection system for smart home IoT devices. *IEEE Internet of Things Journal*, 6(5):9042–9053, 2019.
- [12] O. Brun, Y. Yin, and E. Gelenbe. Deep learning with dense random neural network for detecting attacks against IoT-connected home environments. *Procedia computer science*, 134:458–463, 2018.
- [13] N. Moustafa, B. Turnbull, and K. R. Choo. An ensemble intrusion detection technique based on proposed statistical flow features for protecting network traffic of internet of things. *IEEE IoT Journal*, 6(3):4815–4830, 2018.
- [14] M. Nobakht, V. Sivaraman, and R. Boreli. A host-based intrusion detection and mitigation framework for smart home IoT using openflow. In *ARES*, pages 147–156. IEEE, 2016.
- [15] A. Procopiou, N. Komninos, and C. Douligeris. Forchaos: Real time application DDoS detection using forecasting and chaos theory in smart home IoT network. *Wireless Communications and Mobile Computing*, 2019.
- [16] M. Novák, F. Jakab, and L. Lain. Anomaly detection in

- 1121 user daily patterns in smart-home environment. *J. Sel.*
 1122 *Areas Health Inform*, 3(6):1–11, 2013.
- 1123 [17] S. Ramapatruni, S. N. Narayanan, S. Mittal, A. Joshi,
 1124 K. P. Joshi, et al. Anomaly detection models for smart
 1125 home security. In *IEEE BigDataSecurity*, 2019.
- 1126 [18] M. Yamauchi, Y. Ohsita, M. Murata, K. Ueda, and
 1127 Y. Kato. Anomaly detection in smart home operation
 1128 from user behaviors and home conditions. *IEEE Trans.*
 1129 *Consumer Electronics*, 66(2):183–192, 2020.
- 1130 [19] A. Acar, H. Fereidooni, T. Abera, A.K. Sikder, M. Mi-
 1131 ettinen, H. Aksu, M. Conti, A.R. Sadeghi, and A.S.
 1132 Uluagac. Peek-a-boo: I see your smart home activities,
 1133 even encrypted! *arXiv preprint arXiv:1808.02741*, 2018.
- 1134 [20] R. Trimananda, J. Varmarken, A. Markopoulou, and
 1135 B. Demsky. Packet-level signatures for smart home
 1136 devices. *Signature*, 10(13):54, 2020.
- 1137 [21] Y. Wan, K. Xu, G. Xue, and F. Wang. IoTArgos: A
 1138 multi-layer security monitoring system for internet-of-
 1139 things in smart homes. In *INFOCOM*, pages 874–883.
 1140 IEEE, 2020.
- 1141 [22] E. Anthi, S. Ahmad, O. Rana, G. Theodorakopoulos, and
 1142 P. Burnap. EclipseIoT: A secure and adaptive hub for the
 1143 Internet of Things. *Comp. & Security*, 78:477–490, 2018.
- 1144 [23] M. Yamauchi, Y. Ohsita, M. Murata, K. Ueda, and
 1145 Y. Kato. Anomaly detection for smart home based on
 1146 user behavior. In *ICCE*, pages 1–6. IEEE, 2019.
- 1147 [24] Google Inc. HTTPS encryption on the web, 2019. URL
 1148 <https://transparencyreport.google.com/https/>.
- 1149 [25] G. Loukas, Y. Yoon, G. Sakellari, T. Vuong, and
 1150 R. Heartfield. Computation offloading of a vehicle’s
 1151 continuous intrusion detection workload for energy ef-
 1152 ficiency and performance. *SIMPAT*, 73:83–94, 2017.
- 1153 [26] F.T. Liu, K.M. Ting, and Z. Zhou. Isolation forest.
 1154 In *2008 Eighth IEEE International Conference on Data*
 1155 *Mining*, pages 413–422. IEEE, 2008.
- 1156 [27] B. Scholkopf, R.C. Williamson, A.J. Smola, J. Shawe-
 1157 Taylor, and J.C. Platt. Support vector method for novelty
 1158 detection. In *Proceedings of the 12th International*
 1159 *Conference on Neural Information Processing*, pages
 1160 582–588. ACM, 2999.
- 1161 [28] D. Tax and R. Duin. Support vector data description.
 1162 *Machine Learning*, 54(1):45–66, 2004.
- 1163 [29] D. Mutz, F. Valeur, G. Vigna, and C. Kruegel. Anomalous
 1164 system call detection. *ACM Transactions on Information*
 1165 *and System Security*, 9(1):61–93, 2006.
- 1166 [30] S. M. Beyer, B. E. Mullins, S. R. Graham, and J. M.
 1167 Bindewald. Pattern-of-life modeling in smart homes.
 1168 *IEEE Internet of Things Journal*, 5(6):5317–5325, 2018.
- 1169 [31] M. N. Katehakis and A. F. Veinott. The multi-armed
 1170 bandit problem: decomposition and computation. *Math-*
 1171 *ematics of Operations Research*, 12(2):262–268, 1987.
- 1172 [32] J. Vermorel and M. Mehryar. Multi-armed bandit algo-
 1173 rithms and empirical evaluation. In *European conference*
 1174 *on machine learning*, pages 437–448. Springer, Berlin,
 1175 Heidelberg, 2005.
- 1176 [33] P. Auer, N. Cesa-Bianchi, Y. Freund, and R. E. Schapire.
 1177 Gambling in a rigged casino: The adversarial multi-
 1178 armed bandit problem. In *Annual Foundations of Com-*
 1179 *puter Science*, pages 322–331. IEEE, 1995. 1179
- [34] R. Seger. rx_tools, 2018. URL [https://github.com/](https://github.com/rxseger/rx_tools) 1180
 rxseger/rx_tools. 1181
- [35] F. Pedregosa et al. Scikit-learn: Machine learning in 1182
 Python. *Journal of Machine Learning Research*, 12: 1183
 2825–2830, 2011. 1184
- [36] P. Auer, N. Cesa-Bianchi, Y. Freund, and R. E. Schapire. 1185
 The nonstochastic multiarmed bandit problem. *SIAM* 1186
journal on computing, 32(1):48–77, 2016. 1187
- [37] L. Kocsis and C. Szepesvári. Discounted UCB. In *2nd* 1188
PASCAL Challenges Workshop, volume 2, 2006. 1189
- [38] R. S. Sutton and A. G. Barto. *Reinforcement learning:* 1190
An introduction. MIT press, 2018. 1191
- [39] L.P. Kaelbling, M.L. Littman, and A.W. Moore. Re- 1192
 inforcement learning: A survey. *Journal of artificial* 1193
intelligence research, 4:237–285, 1996. 1194
- [40] K. Shah. Multi armed bandit algorithms, 2018. URL 1195
[https://github.com/kulinshah98/Multi-Armed-Bandit-](https://github.com/kulinshah98/Multi-Armed-Bandit-Algorithms) 1196
 Algorithms. 1197
- [41] D. Quail. Introduction to reinforcement learning via non- 1198
 stationary bandits, 2017. URL [https://github.com/dquail/](https://github.com/dquail/NonStationaryBandit) 1199
 NonStationaryBandit. 1200
- [42] J. Li, Z. Zhao, R. Li, and H. Zhang. AI-based two-stage 1201
 intrusion detection for software defined iot networks. 1202
IEEE Internet of Things Journal, 6(2):2093–2102, 2018. 1203
- [43] Contiki. The contiki operating system, 2019. URL [https:](https://github.com/contiki-os/contiki/) 1204
[//github.com/contiki-os/contiki/](https://github.com/contiki-os/contiki/). 1205
- [44] Checkmarx. Amazon echo: Alexa leveraged as a silent 1206
 eavesdropper. Technical report, Checkmarx, 10 2018. 1207
 URL <https://info.checkmarx.com/wp-alexa>. 1208
- [45] N. Pitropakis, E. Panaousis, T. Giannetsos, E. Anas- 1209
 tasiadis, and G. Loukas. A taxonomy and survey of 1210
 attacks against machine learning. *Computer Science* 1211
Review, 34, 2019. 1212